Research Square

Preprints are preliminary reports that have not undergone peer review.
They should not be considered conclusive, used to inform clinical practice,
or referenced by the media as validated information.

Development and validation of a thermal analysis model for wire arc directed energy deposition applicable to multiple deposition conditions

Yuta Sugiyama

sugiyama8448641@gmail.com

Tokyo University of Agriculture and Technology: Tokyo Noko Daigaku https://orcid.org/0009-0000-1143-7695

Hiroyuki Sasahara

Tokyo University of Agriculture and Technology: Tokyo Noko Daigaku https://orcid.org/0000-0002-5618-1723

Research Article

Keywords: Wire Arc Directed Energy Deposition (Wire Arc DED), Thermal analysis, Finite element method, Heat transfer modeling, Model calibration, Thermal history prediction

Posted Date: November 9th, 2026

DOI: https://doi.org/10.21203/rs.3.rs-11374210/v1

License: This work is licensed under a Creative Commons Attribution 4.0 International License.
Read Full License

Development and validation of a thermal analysis model for wire arc directed energy deposition applicable to multiple deposition conditions

Yuta Sugiyama[a], Hiroyuki Sasahara[a]

[a]Tokyo University of Agriculture and Technology, Department of Mechanical Systems Engineering, 2-24-16, Naka-cho, Koganei-shi, Tokyo 184-8588, Japan

Corresponding author: Hiroyuki Sasahara (sasahara@cc.tuat.ac.jp)

Abstract

In metal additive manufacturing, accurate prediction of the temperature field is important because the thermal history during deposition strongly affects microstructural evolution and mechanical properties. However, thermal analysis of wire arc directed energy deposition often requires identification of parameters such as heat source geometry and thermal efficiency for specific deposition conditions, and recalibration after condition changes can limit model applicability. This study focused on heat transfer from the substrate to the supporting system and aimed to develop a model whose parameters, identified under one condition, could be transferred to different conditions without re-identification. Three models with different representations of heat transfer beneath the substrate were constructed. Parameters were identified using measured thermal histories under one condition and applied unchanged to four additional conditions with different wire feed speeds, torch travel speeds, and interlayer cooling times. A model incorporating a virtual thin plate beneath the substrate, which equivalently represented heat capacity and horizontal heat conduction in the supporting system, maintained good prediction accuracy across five conditions without recalibration, with overall root mean squared error values of 4.81–6.73 K. It also achieved accuracy comparable to that of a detailed supporting-system model with a simpler configuration and shorter computation time. Comparison with measured thermal histories at different heights on the deposited wall showed that the model reproduced the overall trend and post-deposition cooling behavior. These results demonstrate that appropriate representation of heat transfer to the supporting system can reduce condition-specific recalibration and enable transfer of model parameters across multiple deposition conditions.

Keywords : Wire Arc Directed Energy Deposition (Wire Arc DED); Thermal analysis; Finite element method; Heat transfer modeling; Model calibration; Thermal history prediction

1. Introduction

Wire arc directed energy deposition (wire arc DED) is a metal additive manufacturing process in which a

three-dimensional geometry is formed by sequentially melting and solidifying wire material using an arc as the heat source. Owing to its high deposition rate, this process has attracted attention as a manufacturing and repair technology for large-scale metallic components. Additionally, the use of an arc as the heat source is advantageous because the equipment is relatively inexpensive [1-2]. On the other hand, wire arc DED involves localized melting and solidification caused by the arc heat source, as well as reheating associated with multilayer deposition. The resulting thermal history within the deposit strongly affects microstructural evolution, mechanical properties, residual stress, and deformation [3-5]. Therefore, accurate understanding and prediction of the temperature field during deposition are important for predicting and controlling deposition quality.

Finite element–based thermal conduction analysis is widely used to evaluate thermal histories during deposition. Numerical analysis enables estimation of the temperature distribution inside the deposit, which is difficult to measure directly using thermocouples or infrared cameras. The obtained thermal histories also provide fundamental information for evaluating cooling rate, interlayer temperature, phase transformation, residual stress, and deformation. Therefore, construction of a thermal analysis model capable of accurately predicting the temperature field is an effective approach for understanding the deposition process and designing deposition conditions. In thermal analysis of wire arc DED, it is necessary to appropriately represent transient heating by a moving heat source, changes in material properties associated with melting and solidification, material addition during multilayer deposition, and heat transfer among the deposit, substrate, fixtures, and surrounding environment. However, accurate prediction of the temperature field remains difficult because many of these factors either have uncertain values or are difficult to represent appropriately in a simplified numerical model [6]. In existing thermal analyses of welding and wire arc DED, the arc heat source is commonly modeled as a volumetric heat source, such as Goldak's double-ellipsoidal heat source. Analysis parameters must also be specified, including heat source geometry, thermal efficiency, temperature-dependent material properties, and boundary conditions such as heat transfer coefficients for convection, radiation, and contact. These parameters are essential for performing the analysis and can also serve as identification parameters used to achieve agreement with experimental results. They are often calibrated to reproduce measured thermal histories, molten-pool geometry, bead geometry, or deformation [6-8]. Using such approaches, previous studies have compared predicted thermal histories at representative points, residual stresses, or deformation with experimental results under the deposition conditions used for calibration and have thereby validated their numerical models [7, 9]. However, validation of thermal histories is often based on a limited number of measurement points and specific deposition conditions, and the reproducibility of thermal histories at multiple locations, as well as the prediction accuracy when calibrated analysis conditions are applied to different deposition conditions, has not been sufficiently investigated. In particular, heat source–related analysis parameters, such as heat source geometry and arc thermal efficiency, can vary depending on wire feed speed, torch travel speed, wire material, and other factors [8, 10-11]. Therefore, when deposition conditions change, the same analysis parameters cannot necessarily be applied directly, and additional calibration or validation may be required. This is one factor limiting the general applicability of thermal analysis models for wire arc DED.

In contrast, heat loss from the bottom surface of the substrate to the fixture or worktable is considered a thermal boundary condition that depends more strongly on the experimental setup, fixing method, and contact condition than on the deposition conditions themselves. Therefore, if this heat-loss path can be represented appropriately, the need to re-identify heat source parameters for each deposition condition may be reduced. In conventional thermal analyses of wire arc DED, heat dissipation from the surfaces of the deposit and substrate is generally represented by convection and radiation to the surrounding atmosphere, whereas the bottom surface of the substrate is often simplified using an adiabatic boundary, constant-

temperature boundary, convective boundary, or an equivalent heat transfer boundary representing contact with the fixture [7, 12-13]. However, in actual deposition experiments, heat is transferred from the bottom surface of the substrate to the fixture or worktable, and this heat transfer condition depends on the fixture geometry, clamping condition, contact surface roughness, thermal deformation, contact pressure, and other factors [12]. Therefore, it is difficult to uniquely determine the heat exchange condition at the bottom surface of the substrate from geometric information alone. In wire arc DED, the temperature field is formed as the supplied heat is transferred to the deposit, substrate, fixtures, and surrounding environment. Therefore, accurate prediction of the temperature field is considered difficult if heat exchange at the bottom surface of the substrate is not appropriately represented.

Accordingly, this study aimed to develop a thermal analysis model for wire arc DED that can maintain a certain level of prediction accuracy under different deposition conditions without re-identifying heat source parameters for each condition when the same supporting system is used. In particular, attention was focused on heat transfer beneath the substrate, which represents an experimental system–specific heat-loss path, and three analysis models with different representations of this heat transfer were constructed. For each model, parameters governing heat transfer beneath the substrate were identified by Bayesian optimization through comparison with measured thermal histories under one deposition condition. The identified parameters were then applied to different deposition conditions without re-identification, and the prediction accuracy of the thermal histories was evaluated without recalibration for each deposition condition. Furthermore, for the model judged to be the most suitable, thermal histories at different heights on the deposited wall surface were directly measured using an infrared camera and compared with the analysis results. This enabled validation of the thermal-history prediction accuracy not only on the substrate but also within the deposited wall.

2. Experimental and numerical methods

2.1 Materials and wire arc DED process

Deposition was performed using the wire arc DED system shown in Fig. 1. The wire arc DED system consists of an industrial robot (ARC Mate 100iD, FANUC Corporation, Japan) and a Cold Metal Transfer (CMT) welding machine (Fronius International GmbH, Austria). Using this system, single-bead wall structures were fabricated by reciprocating the wire-feeding torch. In this study, a low-carbon steel wire (SE-A50, Kobe Steel, Japan) was used as the deposition wire, and an S50C steel plate was used as the substrate. The chemical composition of the wire material is listed in Table 1.

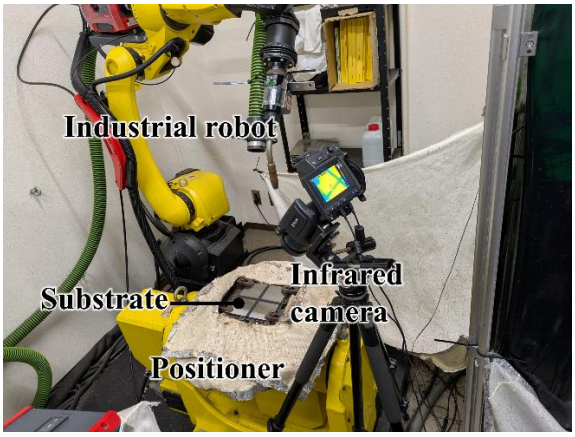


Fig. 1 Wire arc DED system and infrared camera

Table 1 Chemical composition of wire (wt.%)

Wire	C	Si	Mn	P	S	Cr	Fe
SE-A50	0.06	0.62	1.27	0.010	0.015	—	Bal.

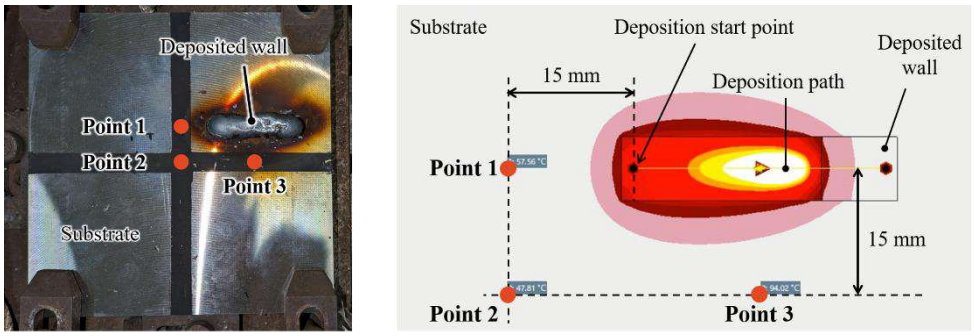
Table 2 Deposition conditions

Condition no.	1	2	3	4	5
Wire	SE-A50				
Substrate	S50C				
Wire feed speed [m/min]	7	7	7	9	5
Torch speed [mm/min]	700	500	900	700	700
Number of layers	10	10	10	10	10
Interlayer cooling time [s]	0	0	10	10	0

Among the deposition conditions listed in Table 2, Condition 1 was used to identify the parameters of the thermal analysis model, whereas Conditions 2–5 were used to evaluate the transferability of the identified parameters. Interlayer cooling was introduced only in Conditions 3 and 4 to prevent excessive sagging of the deposited material.

2.2 Substrate temperature measurement for parameter identification

In this study, the temperature of the substrate surface was measured using the infrared camera shown in Fig. 1 (FLIR T650sc, FLIR Systems, USA) and used as a reference for parameter identification. As shown in Fig. 2(a), blackbody spray was applied in a cross-shaped pattern on the substrate surface, and a wall structure was deposited adjacent to the coated area. Thermal histories were then obtained at the three points shown in Fig. 2 within the blackbody-coated region and compared with the analysis results.



(a) (b)

Fig. 2 (a) Blackbody-coated area on the substrate and (b) locations used for comparison between measured and simulated temperatures

2.3 Thermal analysis model

Numerical analysis was performed using Simufact Welding (version 2025.1, Hexagon, Germany). This welding simulation software can perform thermal and structural analyses using the finite element method. The flow of molten metal is not considered in the software, and the temperature field is calculated based on the heat conduction equation for solids. In addition to calculating the temperature field, structural analysis can be coupled with the thermal analysis to evaluate residual stress and deformation. However, because the objective of this study was to predict thermal histories, only thermal analysis was performed.

In the analysis, the final geometry of the deposit was prepared in advance, and the deposition process was simulated by sequentially activating elements as the heat source moved. In this study, rectangular prisms approximated the deposit's geometry. Log data recorded by the welding machine were used to set the amount of wire fed and the power consumption during deposition in the analysis to the same values as those in the experiments. The arc thermal efficiency was set to 85% [14], and the Goldak double-ellipsoidal heat source model was employed. The heat source geometry was estimated using the estimation function implemented in the software only for Condition 1 listed in Table 2, and the same geometry was used for Conditions 2–5. However, because the elements of the deposit are sequentially activated as the heat source approaches in this software, elements at the bead edges may not be activated if the heat source is too narrow. Therefore, the width of the volumetric heat source was set equal to the bead width under each deposition condition, while all other heat source geometry parameters were kept the same for all deposition conditions.

Material properties of the deposit, substrate, and supporting components, including thermal conductivity, specific heat, and density, were defined based on the material database implemented in Simufact Welding and literature values, with their temperature dependence taken into account. For SE-A50 and S50C, because the database did not contain material data with compositions sufficiently close to those of the actual materials, temperature-dependent material properties were defined based on data for materials with similar chemical compositions and material classifications, also with reference to Refs. [15-16]. The thermophysical properties used for the wire material (SE-A50) and S50C are shown in Fig. 3.

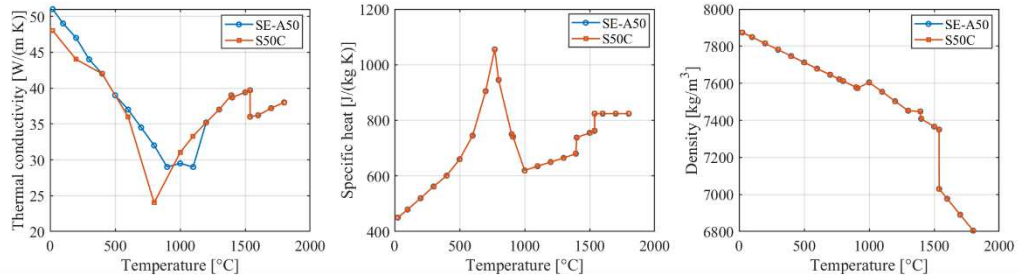


Fig. 3 Temperature-dependent thermophysical properties used for SE-A50 and S50C in the numerical analysis: (a) thermal conductivity, (b) specific heat, and (c) density

The surface heat transfer coefficient and emissivity representing heat loss to the surrounding atmosphere were assumed to be independent of temperature and were set to constant values of 20 W/(m² K) and 0.28, respectively. In addition, the contact area between the deposit and the substrate, defined as the cross-sectional area of the deposit at z = 0, was measured using a 3D scanner (VL-300, Keyence Corporation, Japan) and set to match the actual contact area.

The three thermal analysis models shown in Fig. 4(a) were constructed and compared. Model I was developed with reference to simplified boundary conditions commonly used in conventional thermal analyses of wire arc DED [6-7]. In this model, the substrate was placed on a plate maintained at a constant temperature (backing plate). Heat transfer across the contact interface between the bottom surface of the substrate and the backing plate was defined based on the temperature difference between the two components and the contact heat transfer coefficient. Model II is the model newly proposed in this study. In this model, a virtual plate with a thickness of 2 mm and the same planar area as the substrate (hereafter referred to as Plate I) was inserted between the substrate and the plate used in Model I. Plate I does not represent any specific physical material but was introduced as a virtual domain providing an equivalent representation of heat transfer from the bottom surface of the substrate to the supporting system, including heat conduction in both the vertical and horizontal directions. Therefore, the thermal conductivity and specific heat of Plate I were not assigned as properties of a specific material but were treated as parameters to be identified to provide an equivalent representation of the heat capacity and heat diffusion of the supporting system beneath the substrate. These parameters were treated as effective values representing the thermal characteristics of the supporting system. The density of Plate I was set to 7850 kg/m³. The contact heat transfer coefficient at the interfaces between components was also treated as a parameter to be identified to reproduce the thermal response of the experimental system. Finally, Model III reproduced the actual experimental setup shown in Fig. 4(b) as closely as possible, including the two plates located beneath the substrate. A 5000-series aluminum alloy plate (Plate II), 10 mm thick and having the same planar area as the substrate, was placed directly beneath the substrate. Below Plate II, a stainless-steel plate (Plate III) with a thickness of 20 mm and an area of 600 cm² (20 cm × 30 cm) was installed.

For all models, the mesh size within the deposit was set to 0.5 mm in the horizontal direction. In the z-direction, each layer was divided into two or three elements so that the element shape was as close to cubic as possible. The mesh sizes of the other components were set as listed in Table 3.

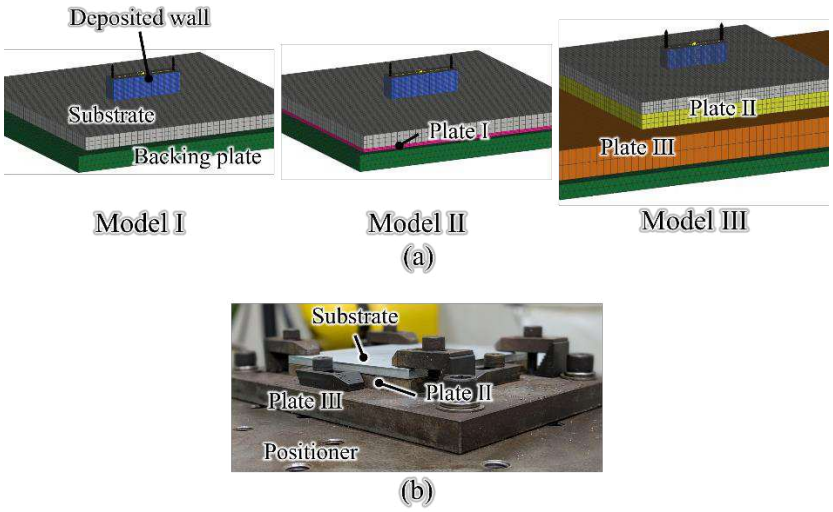


Fig. 4 (a) Schematic overview of the analysis models and
(b) experimental setup used for model development

Table 3 Approximate element dimensions of each component in the analysis models

Model no.	Component	Approximate element dimensions [mm]
I	Substrate	2 × 2 × 2.67
II	Substrate	2 × 2 × 2.67
	Plate I	1 × 1 × 0.67
III	Substrate	2 × 2 × 2.67
	Plate II	4 × 4 × 3.33
	Plate III	7.5 × 7.5 × 6.67

In thermal analysis of wire arc DED, identification of analysis parameters related to heat input is often emphasized, while the boundary condition at the bottom surface of the substrate is frequently simplified, as in conventional models [6-7]. To achieve highly accurate prediction of thermal histories, it is desirable to adjust the heat input–related parameters according to the deposition conditions; however, re-identifying these parameters for each deposition condition increases the analysis cost. Therefore, in all three models considered in this study, calibration was performed using parameters associated with the supporting system that do not directly depend on the deposition conditions, such as the boundary conditions and the material properties of the plates placed beneath the substrate. The aim was thus to construct an analysis model capable of maintaining a certain level of prediction accuracy under different deposition conditions without re-identifying the heat input–related parameters for each condition. Numerical analyses were performed on a PC equipped with an Intel Core i7-10700 processor (2.90 GHz, 8 cores) and 16 GB of RAM.

2.4 Temperature measurement of the deposited wall for validation of predicted thermal histories

In this study, blackbody spray was applied to the measurement locations on the substrate to reduce the influence of emissivity and obtain high-accuracy temperature measurements, and the resulting thermal histories were compared with the analysis results. However, although this method enables direct validation of the thermal histories on the substrate, it does not allow direct evaluation of the prediction accuracy of the thermal histories within the deposit itself. Therefore, the temperature of the deposit was also measured using an infrared camera and compared with the thermal histories obtained from the analysis.

Before the temperature of the deposit was measured, the emissivity of the deposit surface was identified using the temperature of the blackbody-coated region as a reference. Specifically, the thermal history obtained from the blackbody-coated region was used as the reference, and the root mean squared error (RMSE) was calculated for the thermal histories measured in the uncoated region while varying the emissivity from 0.74 to 0.81 in increments of 0.01. As a result, an emissivity of 0.79, which yielded the minimum RMSE, was adopted as the emissivity of the deposit surface. The RMSE evaluation was performed over the temperature range of 50–100 °C.

When measuring the temperature on the side surface of the deposit, it is desirable to ensure sufficient build height because measurements should be taken from a direction as nearly perpendicular to the wall surface as possible. Therefore, in this validation experiment, the wire feed speed was set to a relatively high value and an interlayer cooling time was introduced, resulting in the fabrication of a 20-layer wall structure. Although the emissivity of the deposit surface was treated as a constant value in this measurement, the actual emissivity may vary depending on temperature and surface condition [17-18]. In addition, it is difficult to obtain thermal histories from exactly the same locations in the experiment and numerical analysis. Therefore, comparisons between the measured and simulated temperatures on the deposit surface should be interpreted with consideration of the uncertainties associated with emissivity and spatial correspondence.

Table 4 Deposition conditions for validation of the thermal analysis model

Wire	SE-A50
Substrate	S50C
Wire feed speed [m/min]	9
Torch speed [mm/min]	700
Number of layers	20
Interlayer cooling time [s]	10

3. Model calibration

3.1 Parameter identification

The parameters of each model were identified using the temperature measurements obtained under Condition 1 listed in Table 2. In Model I, only the contact heat transfer coefficient was identified. In Model II, the parameter set comprised three variables: a single contact heat transfer coefficient applied to the interfaces between all components, the thermal conductivity of the virtual Plate I, and its specific heat. In Model III, a single contact heat transfer coefficient applied to the interfaces between all components was the only parameter identified. Bayesian optimization was used for this purpose. In the Bayesian optimization procedure, conditions predicted to reduce the value of the objective function were sequentially selected based on the analysis results obtained at the initial evaluation points. Table 5 summarizes the parameters, their search ranges, the number of initial evaluation points, and the number of additional evaluations performed by Bayesian optimization for each model.

Table 5 Parameter settings for Bayesian optimization

Model	Parameter	Search range	Number of initial evaluations	Number of additional evaluations
I	Contact heat transfer coefficient [W/(m² K)]	1-10⁶	4	8
II	Contact heat transfer coefficient [W/(m² K)]	1-10⁶	10	30
	Specific heat of Plate I [J/(kg K)]	1-5000		
	Thermal conductivity of plate I [W/(m K)]	100-500		
III	Contact heat transfer coefficient [W/(m² K)]	1-10⁶	4	8

For parameter identification in each model, the RMSE between the simulated and measured thermal histories was used as the evaluation metric. The simulated and measured temperatures were linearly interpolated to obtain temperature values at 0.1 s intervals. For each deposition condition, the evaluation period was defined as extending from the start of deposition to 60 s after the end of deposition. The RMSE was calculated at each of the three temperature measurement points from the differences between the simulated and measured values at each evaluation time. To comprehensively evaluate the errors at the three measurement points, the overall RMSE was calculated from the RMSE values at the individual points using Eq. (1), and this value was minimized as the objective function for parameter identification.

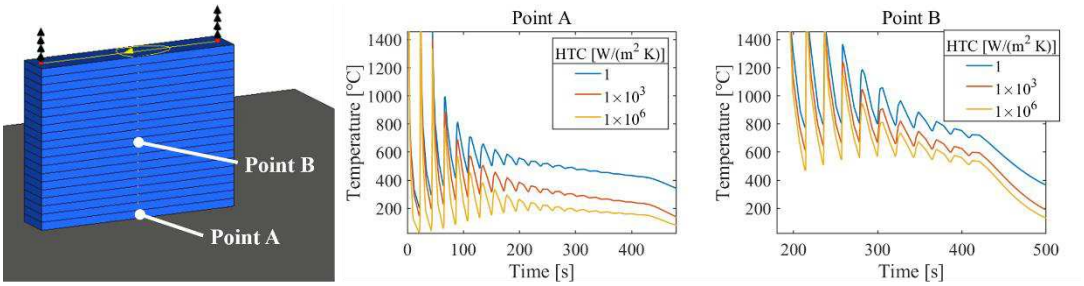
$$Overall\ RMSE = \sqrt{\frac{RMSE_1^2 + RMSE_2^2 + RMSE_3^2}{3}} \tag{1}$$

Because it is difficult to explicitly formulate in advance the relationships among the identification variables, the thermal histories obtained from the analyses, and the overall RMSE calculated from them, parameter identification was approached through black-box optimization. Bayesian optimization is well suited to this type of problem and was employed to efficiently search for the optimal combination of variables within a limited number of analysis runs, particularly for Model II, in which multiple variables had to be identified

simultaneously.

3.2 Effect of heat transfer beneath the substrate on thermal history

The effect of heat transfer beneath the substrate, which is the focus of this study, on the thermal history of the deposit was investigated. As an example, the effect of varying the contact heat transfer coefficient between the bottom surface of the substrate and the backing plate in Model I was examined. Figure 5 shows the locations at which the thermal histories were evaluated and the thermal histories obtained at each location when the contact heat transfer coefficient was varied over a wide range. The results shown here correspond to the analysis of the deposition condition used for temperature measurement of the deposit, as listed in Table 4.



(a) (b) (c)

Fig. 5 Effect of contact heat transfer coefficient (HTC) on thermal histories at different heights on the deposited wall: (a) evaluation positions, (b) Point A near the wall base, and (c) Point B at mid-height. The legend indicates the HTC values in W/(m² K)

As the contact heat transfer coefficient increased, heat transfer from the bottom surface of the substrate to the backing plate increased, resulting in a substantial decrease in the temperature within the deposit. This indicates that, to accurately predict the thermal history within the deposit, it is important to appropriately represent not only the heat source conditions but also heat transfer beneath the substrate.

In thermal analysis of metal additive manufacturing, parameters related to heat input, such as the geometry of the volumetric heat source and arc thermal efficiency, have a significant influence on prediction accuracy and are therefore often treated as parameters to be identified [6-8]. Heat transfer beneath the substrate, on the other hand, depends on the contact condition between the substrate and the supporting components, as well as on the configuration of the supporting system, and the predicted thermal history can therefore also vary depending on how this heat transfer is represented.

In this study, attention was focused on the representation of heat transfer beneath the substrate. If the configuration of the supporting system remains unchanged, the supporting system itself essentially remains the same even when the deposition conditions are changed. Therefore, if heat transfer beneath the substrate can be modeled appropriately, the same model parameters may be applicable without re-identifying the

parameters associated with this part of the model for each deposition condition. This is considered important for improving the applicability of the thermal analysis model to different deposition conditions.

4. Results and discussion

4.1 Model I

The contact heat transfer coefficient was the only parameter to be identified in this model, and the overall RMSE reached its minimum value when the coefficient was 754 W/(m² K). Figure 6 compares the analysis results under the optimal condition with the measured temperature histories. The discrepancy between the measured and simulated results was large, and the cooling rate after deposition also differed substantially from the measured value. The overall RMSE for this result was 21.68 K.

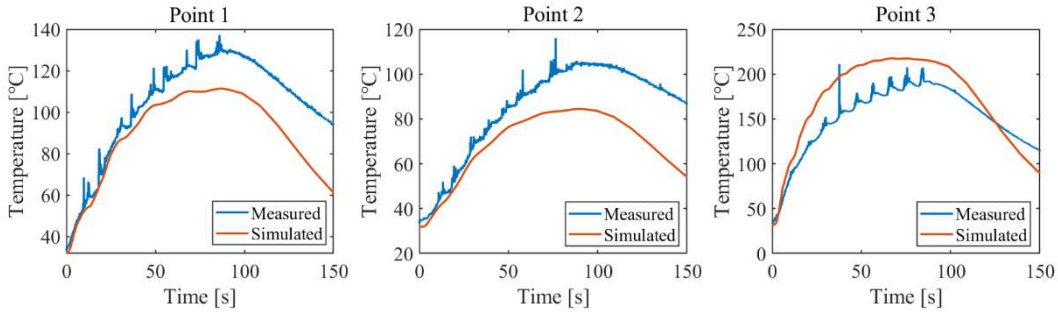


Fig. 6 Comparison of simulated and measured temperature histories for calibrated Model I (HTC = 754 W/(m² K))

Table 6 shows the RMSE values for Conditions 1–5. For Conditions 2–5, the parameters calibrated under Condition 1 were applied without re-identification. The errors were large at all three measurement points under all conditions, indicating that high-accuracy temperature prediction was not achieved.

Table 6 RMSE between calculated and measured temperature histories for Model I

Condition no.	Point 1 RMSE [K]	Point 2 RMSE [K]	Point 3 RMSE [K]	Overall RMSE [K]
1	17.17	18.32	27.92	21.68
2	21.77	24.90	18.82	21.97
3	14.08	15.07	31.33	21.66
4	14.09	15.80	25.01	18.92
5	23.81	23.78	15.77	21.46

4.2 Model II

The parameters to be identified in this model were the contact heat transfer coefficient, the specific heat of virtual Plate I, and its thermal conductivity. The overall RMSE reached its minimum value when these parameters took the values listed in Table 7. Figure 7 compares the analysis results under the optimal condition with the measured temperature histories. In contrast to Model I, the simulated temperatures at all

measurement points showed good agreement with the measured results, including the cooling behavior after deposition, and the overall RMSE was 4.81 K.

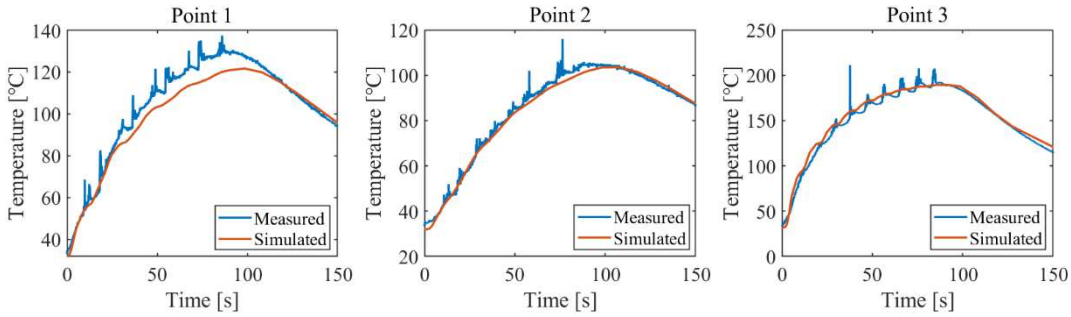


Fig. 7 Comparison of simulated and measured temperature histories for calibrated Model II using the parameters listed in Table 7

Table 7 Identified parameters for Model II

Parameter	Identified value
Contact heat transfer coefficient [W/(m² K)]	469
Specific heat of plate Ⅰ [J/(kg K)]	1086
Thermal conductivity of plate Ⅰ [W/(m K)]	386

Table 8 shows the RMSE values for Conditions 1–5 using the parameters identified under Condition 1. The simulated temperatures at each measurement point showed good agreement with the measured values, and good prediction accuracy was maintained for Conditions 2–5.

Table 8 RMSE between calculated and measured temperature histories for Model II

Condition no.	Point 1 RMSE [K]	Point 2 RMSE [K]	Point 3 RMSE [K]	Overall RMSE [K]
1	6.16	1.96	5.26	4.81
2	2.99	2.33	8.07	5.15
3	3.34	1.94	10.27	6.34
4	3.83	3.27	10.51	6.73
5	2.29	1.73	8.54	5.20

4.3 Model III

The contact heat transfer coefficient was the only parameter to be identified in this model, and the overall RMSE reached its minimum value when the coefficient was 4480 W/(m² K). Figure 8 compares the analysis results under the optimal condition with the measured temperature histories. As in Model II, the simulated temperatures at each measurement point showed good agreement with the measured results, including the cooling behavior after deposition, and the overall RMSE was 6.43 K.

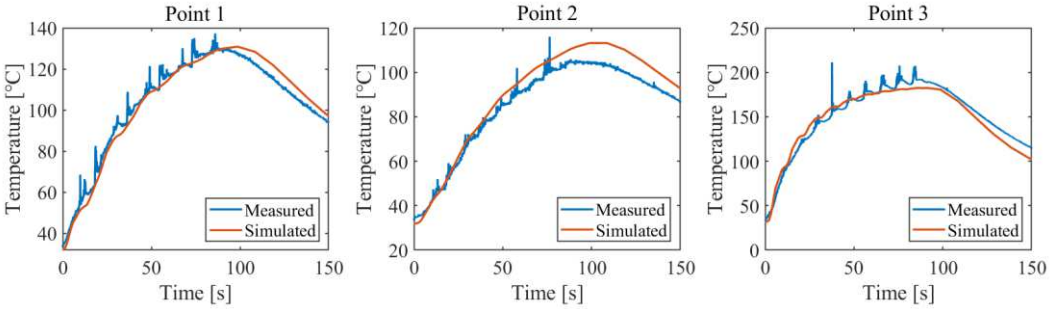


Fig. 8 Comparison of simulated and measured temperature histories for calibrated Model III (HTC = 4480 W/(m² K))

Table 9 shows the RMSE values for Conditions 1–5 using the parameters identified under Condition 1. The simulated temperatures at each measurement point showed good agreement with the measured values, and good prediction accuracy was maintained for Conditions 2–5.

Table 9 RMSE between calculated and measured temperature histories for Model III

Condition no.	Point 1 RMSE [K]	Point 2 RMSE [K]	Point 3 RMSE [K]	Overall RMSE [K]
1	4.20	6.30	8.18	6.43
2	5.04	5.83	6.67	5.89
3	4.62	5.90	8.59	6.58
4	6.88	8.79	4.81	7.02
5	2.16	5.07	12.52	7.90

4.4 Comparison of the three models

Figure 9(a) shows the overall RMSE values for all models and all deposition conditions. The results indicate that both Model II and Model III exhibited low overall RMSE values across multiple deposition conditions, demonstrating that high-accuracy prediction of thermal histories was possible. On the other hand, because Model III reproduced the supporting components of the experimental system in greater detail, its computation time was longer than that of Model II, as shown in Fig. 9(b). In contrast, Model II achieved a shorter computation time while maintaining prediction accuracy comparable to that of Model III. Therefore, among the three models compared in this study, Model II was considered the most suitable in terms of both prediction accuracy and computational cost. The computation times shown in Fig. 9(b) were obtained by running each analysis case individually on the same PC to compare the computational loads of the models under the same conditions.

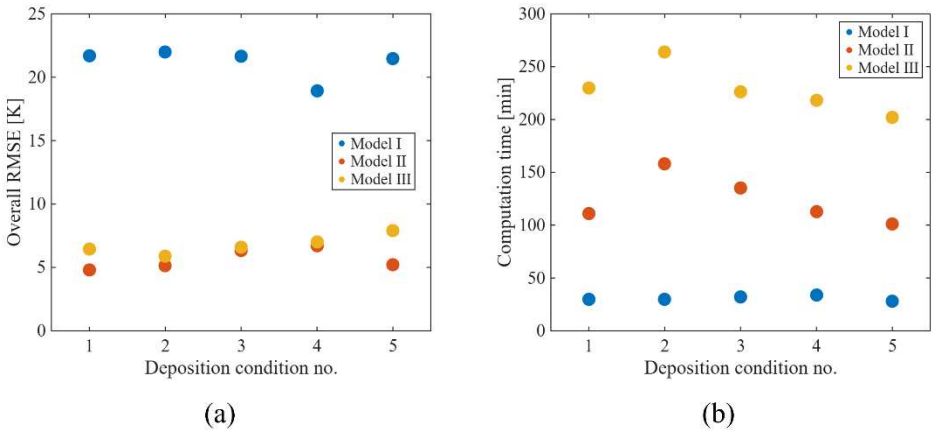


Fig. 9 Comparison of prediction accuracy and computation time among the thermal analysis models: (a) overall RMSE under different deposition conditions and (b) computation time

4.5 Mechanism of improved prediction by Model II

This section discusses why Model II achieved high-accuracy thermal analysis while maintaining a relatively low computational cost. In Model I, the errors were large under all deposition conditions, and the temperature at Point 3 was higher than the measured value, as shown in Fig. 6. The same tendency was observed under all deposition conditions. In Model I, a spatially uniform contact heat transfer coefficient was assigned to the interface between the bottom surface of the substrate and the backing plate, and the temperature of the backing plate was held constant at all locations. Therefore, horizontal heat diffusion occurring within the actual supporting system could not be represented. In the actual supporting system, however, heat transferred from the substrate is conducted not only in the vertical direction but also in the horizontal direction within the supporting components. Therefore, horizontal heat diffusion within the supporting system is also considered to affect the temperature differences among the measurement points on the substrate surface.

In Model I, because the temperature of the backing plate in contact with the bottom surface of the substrate is constant at all locations, horizontal heat transfer within the supporting system cannot be represented, and horizontal heat diffusion occurs only within the substrate. As a result, the temperatures at points relatively far from the heat input location tend to increase less. The temperature tended to rise more readily at Point 3 than at Points 1 and 2. When the model parameters were optimized to minimize the errors, including those at these points, the model overpredicted the temperature at Point 3 and underpredicted the temperatures at Points 1 and 2.

Therefore, to accurately reproduce the temperatures at all three points, it is considered important to appropriately redistribute heat in the horizontal direction so that the temperature differences among the three points are properly represented. In Model II, the heat flux on the cross section through the center of

the deposit shown in Fig. 10(a) indicates that heat entering the virtual Plate I is transferred in the horizontal direction. This horizontal heat transfer increased the temperature beneath the substrate at locations farther from the heat input region and consequently increased the substrate surface temperature at those locations. As a result, the temperature differences among the three points were better reproduced, which is considered to have contributed to the improved prediction accuracy.

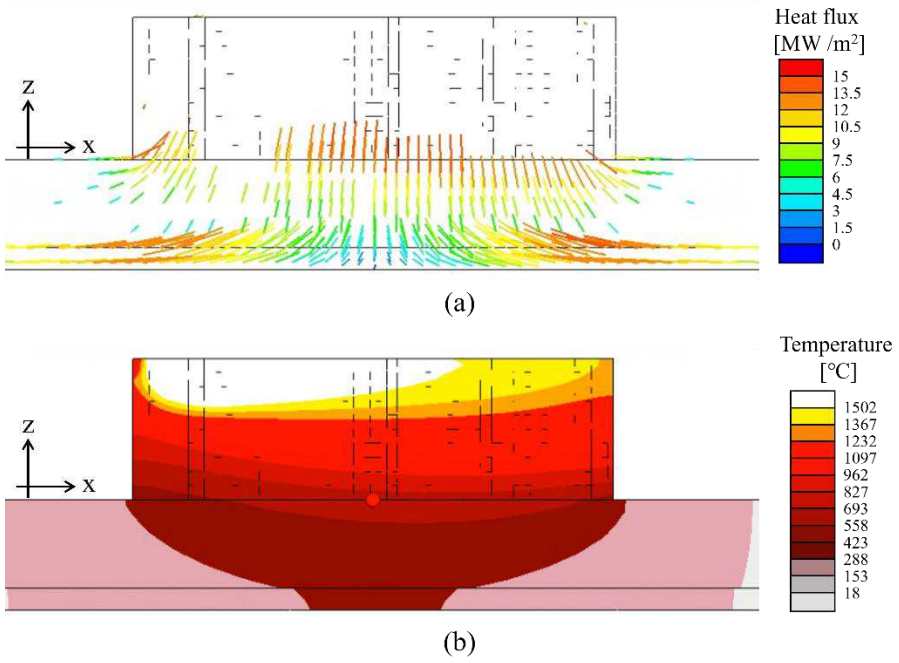


Fig. 10 Heat flux (a) and temperature distribution (b) in the cross section of the deposited wall immediately after deposition of the 10th layer for Model II

5. Validation of predicted thermal histories on the deposited wall surface

For Model II, which was determined to be the most suitable analysis model, the temperature of the deposit surface was measured to directly validate the prediction accuracy of the thermal histories on the deposit surface. Figure 11 compares the measured and simulated thermal histories at surface positions corresponding to the 1st, 8th, and 16th deposited layers. Table 10 summarizes the RMSE and mean absolute error (MAE) between the measured and simulated results at each position.

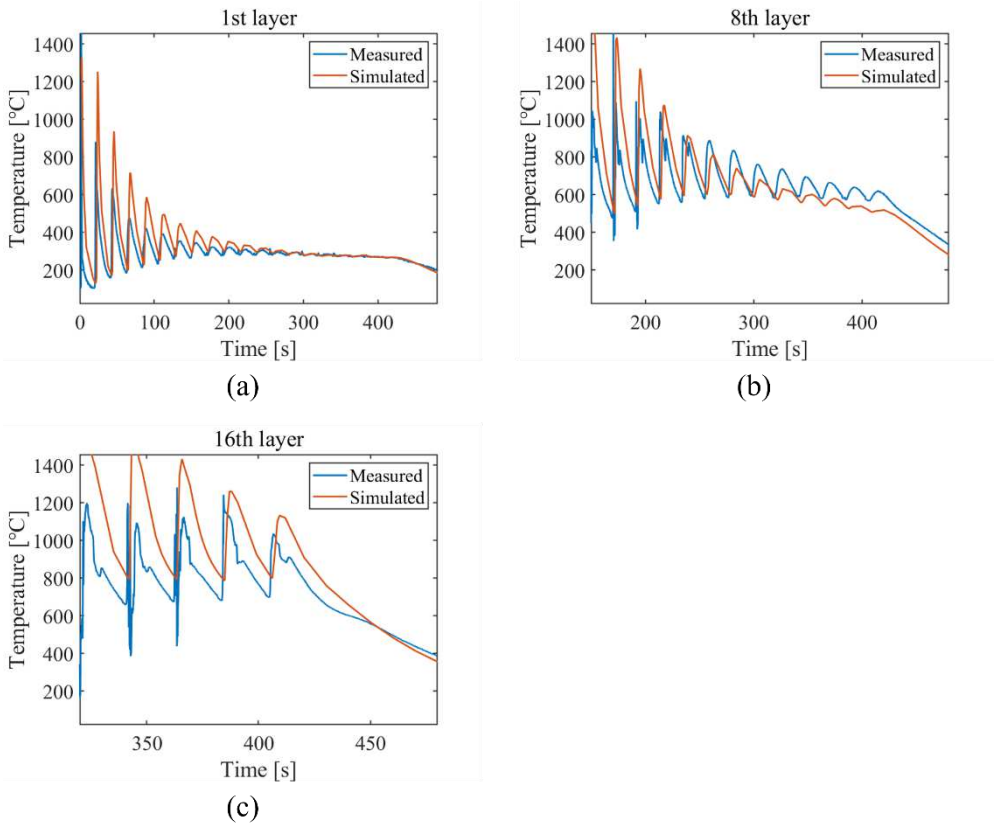


Fig. 11 Comparison of measured and predicted thermal histories at different surface positions on the deposited wall: (a) 1st layer, (b) 8th layer, and (c) 16th layer

Table 10 Prediction errors between measured and simulated surface temperature histories at different heights on the deposited wall

Position	RMSE [K]	MAE [K]
1st layer	69.54	37.27
8th layer	99.84	78.84
16th layer	156.13	119.52

At all measurement positions, the analysis results reproduced the overall trend of the measured thermal histories. In particular, the minimum temperatures reached after deposition of each layer and the cooling behavior after completion of deposition showed generally good agreement between the analysis and measurements. In contrast, the discrepancy between the two became relatively large in the high-temperature range. In this study, the emissivity of the deposit surface was treated as a constant value in temperature measurements using an infrared camera. However, the emissivity of metals has been reported to vary with temperature and surface condition, including oxidation state [17-18]. Because the emissivity identified over the temperature range of 50–100 °C was applied over the entire measurement range in this study, the actual

emissivity may have differed from the assumed value at higher temperatures, which is considered to have contributed to measurement error. In addition, the thermal analysis used in this study did not account for molten metal flow, and the temperature field was calculated based on the heat conduction equation for solids. Therefore, near the molten pool, where heat transport due to molten metal flow can be significant, errors arising from this modeling approximation may also become relatively large. Accordingly, the discrepancy between the simulated and measured temperatures in the high-temperature range may have been affected by both measurement uncertainty associated with the emissivity setting and the simplified representation of heat transport near the molten pool in the analysis model.

On the other hand, the thermal histories during cooling were predicted relatively well. In wire arc DED, these thermal histories provide important information for evaluating cooling rates and phase transformation behavior. Therefore, when these aspects are the primary evaluation targets, Model II, proposed in this study, may reduce the need for recalibration for each deposition condition.

However, as shown in Table 10, both RMSE and MAE increased with increasing height. At higher positions, the influence of heat transfer beneath the substrate on the local thermal history becomes relatively smaller, and the corrective effect of the parameters associated with the supporting system identified in this study may also decrease. Therefore, at higher positions, the influence of analysis conditions other than those associated with the supporting system, such as heat source geometry and local heat input distribution, may become relatively more significant. These results indicate that Model II can reproduce the overall trend of the thermal history and the post-deposition cooling behavior on the deposit surface, while further improvement is required for quantitative agreement at higher positions, particularly in the high-temperature range during deposition.

6. Conclusion

Heat transfer from the bottom surface of the substrate to the supporting system was investigated to enable model parameters identified under a single deposition condition to be transferred to different deposition conditions without condition-specific re-identification. Model II, which introduced a virtual thin plate beneath the substrate to provide an equivalent representation of the heat capacity and horizontal heat conduction of the supporting system, achieved prediction accuracy comparable to that of the detailed Model III while requiring a simpler model configuration and shorter computation time. The identified parameters also maintained good prediction accuracy when applied to deposition conditions with different wire feed speeds, torch travel speeds, and interlayer cooling times, including conditions with different heat inputs per unit bead length. These results demonstrate that appropriate representation of heat transfer through the supporting system can improve parameter transferability across different thermal conditions without recalibration for each condition.

For Model II, a comparison with measured thermal histories at different heights on the deposit surface showed that the model generally reproduced the overall temperature-history trend and post-deposition cooling behavior. However, larger discrepancies were observed both in the high-temperature range and at

higher positions. The discrepancies in the high-temperature range may be mainly associated with measurement uncertainty caused by the emissivity setting, whereas those at higher positions may be related to the reduced influence of the supporting-system boundary condition and the relatively greater influence of heat source–related factors such as heat source geometry and local heat input distribution. Overall, Model II provides a simplified thermal analysis framework that reduces the need for condition-dependent recalibration while maintaining applicability across multiple deposition conditions.

References

[1] Yamagata Y, Sakurai Y, Nitawaki M, Sagawa T, Abe T, Kaneko J, Ko S (2025) Experimental study on thickness control and structural performance of aluminum alloy stub columns fabricated via directed energy deposition-arc. Mech Eng J 12(5):25-00220. https://doi.org/10.1299/mej.25-00220

[2] Du X, Shen Y, Zhao W, Chen J, Liu R, Wei Y (2023) Wire arc additive manufacturing from the perspective of remanufacturing: a review of data processing. J Manuf Process 107:385–410. https://doi.org/10.1016/j.jmapro.2023.10.019

[3] Rodrigues TA, Duarte V, Miranda RM, Santos TG, Oliveira JP (2019) Current status and perspectives on wire and arc additive manufacturing (WAAM). Materials 12(7):1121. https://doi.org/10.3390/ma12071121

[4] Rosli NA, Alkahari MR, Abdollah MF, Maidin S, Ramli FR, Herawan SG (2021) Review on effect of heat input for wire arc additive manufacturing process. J Mater Res Technol 11:2127–2145. https://doi.org/10.1016/j.jmrt.2021.02.002

[5] Gurmesa FD, Lemu HG (2023) Literature review on thermomechanical modelling and analysis of residual stress effects in wire arc additive manufacturing. Metals 13(3):526. https://doi.org/10.3390/met13030526

[6] Sampaio RFV, Pragana JPM, Bragança IMF, Silva CMA, Nielsen CV, Martins PAF (2023) Modelling of wire-arc additive manufacturing – a review. Adv Ind Manuf Eng 6:100121. https://doi.org/10.1016/j.aime.2023.100121

[7] Graf M, Hälsig A, Höfer K, Awiszus B, Mayr P (2018) Thermo-mechanical modelling of wire-arc additive manufacturing (WAAM) of semi-finished products. Metals 8(12):1009. https://doi.org/10.3390/met8121009

[8] Kik T (2024) Calibration of heat source models in numerical simulations of welding processes. Metals 14(11):1213. https://doi.org/10.3390/met14111213

[9] Ding J, Colegrove P, Mehnen J, Ganguly S, Sequeira Almeida PM, Wang F, Williams S (2011) Thermo-mechanical analysis of wire and arc additive layer manufacturing process on large multi-layer parts. Comput Mater Sci 50(12):3315–3322. https://doi.org/10.1016/j.commatsci.2011.06.023

[10] Kollár D, Kövesdi B (2019) Validation of heat source model for metal active gas welding. In: Sommitsch C, Enzinger N, Mayr P (eds) Mathematical Modelling of Weld Phenomena 12. Verlag der Technischen Universität Graz, Graz. https://doi.org/10.3217/978-3-85125-615-4-05

[11] Grossi N, Pierattini G, Morelli L, Scippa A (2026) Dot-by-dot wire arc additive manufacturing geometry prediction: an analytical model. Int J Adv Manuf Technol. https://doi.org/10.1007/s00170-026-19069-3

[12] Czipin M, Wenda A, Hartl K, Akalin E, Stockinger M (2025) Thermo mechanical finite element analysis of the plasma wire arc additive manufacturing process in DEFORM® 13. J Adv Join Process 12:100321. https://doi.org/10.1016/j.jajp.2025.100321

[13] Lee SH (2020) CMT-based wire arc additive manufacturing using 316L stainless steel: effect of heat accumulation on the multi-layer deposits. Metals 10(2):278. https://doi.org/10.3390/met10020278

[14] Pépe N, Egerland S, Colegrove PA, Yapp D, Leonhartsberger A, Scotti A (2011) Measuring the process efficiency of controlled gas metal arc welding processes. Sci Technol Weld Join 16(5):412–417. https://doi.org/10.1179/1362171810Y.0000000029

[15] Hwang JK (2024) Comparison of thermal behaviors of carbon and stainless steel billets during the heating process. Materials 17(1):183. https://doi.org/10.3390/ma17010183

[16] Jimbo I, Cramb AW (1993) The density of liquid iron-carbon alloys. Metall Trans B 24(1):5–10. https://doi.org/10.1007/BF02657866

[17] de Deus VS, de Castro JA, Corrêa SRR (2020) Prediction of the emissivity curve at high temperatures of low carbon steel. J Mater Sci Res 9(2):59–70. https://doi.org/10.5539/jmsr.v9n2p59

[18] Shi D, Zou F, Zhu Z, Sun J (2015) Effect of surface oxidization on the normal spectral emissivity of straight carbon steel at 800–1100 K in air. ISIJ Int 55(3):697–705. https://doi.org/10.2355/isijinternational.55.697

Declarations

Funding

This work was partly supported by JSPS KAKENHI Grant Numbers JP23K26010 and JP26K00844.

Competing Interests

The authors have no relevant financial or non-financial interests to disclose.

Credit authorship contribution statement

Yuta Sugiyama : Conceptualization, Methodology, Validation, Formal analysis, Investigation, Writing – original draft, Visualization

Hiroyuki Sasahara : Methodology, Resources, Writing – review & editing, Supervision, Project administration, Funding acquisition